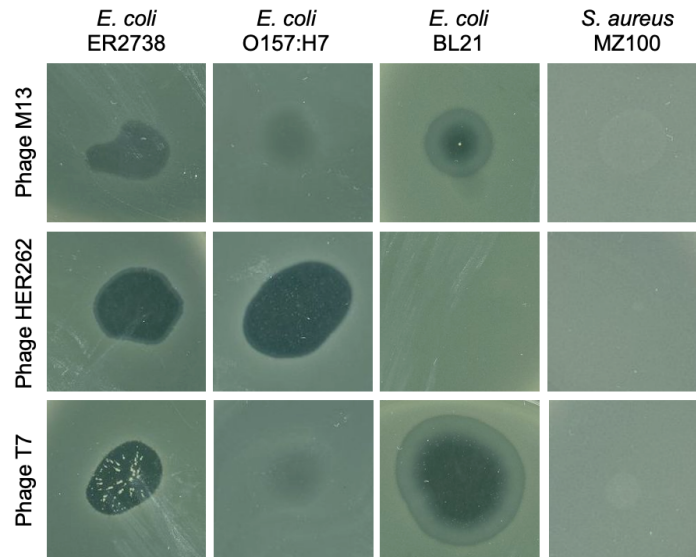


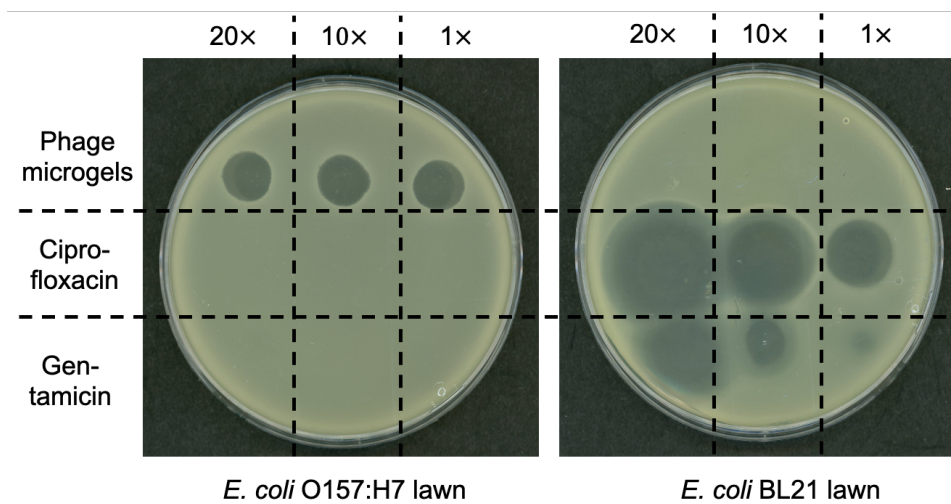
High-throughput fabrication of antimicrobial phage microgels and example applications in food decontamination

In the format provided by the authors and unedited

Supplementary information

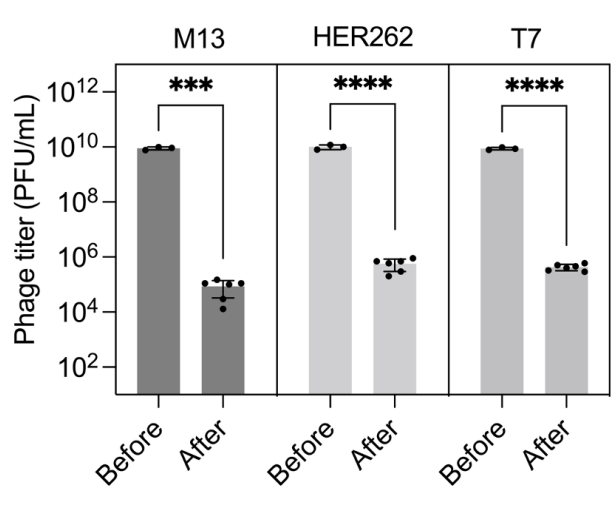


Supplementary Figure 1. Specific bacteria-killing of phage M13, HER262 and T7. Spot test of phage M13, HER262 and T7 on the lawn of *E. coli* ER2738, O157:H7, BL21, and *S. aureus* MZ100, respectively. Image adapted with permission from ref.¹, Nature Portfolio.

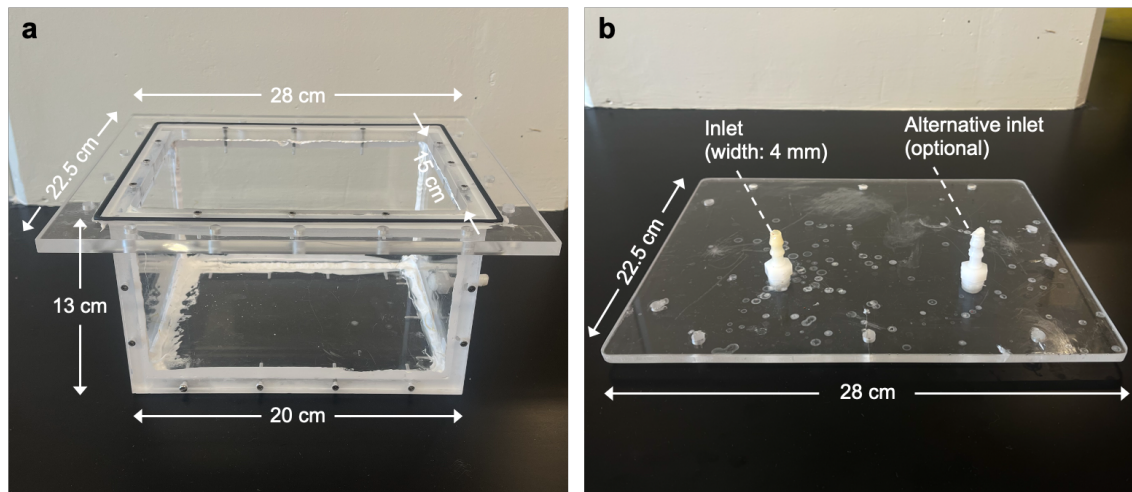


Supplementary Figure 2. Comparison of antimicrobial function of M13+HER262+BSA+GA microgels and representative antibiotics (ciprofloxacin and gentamicin). Spot test of

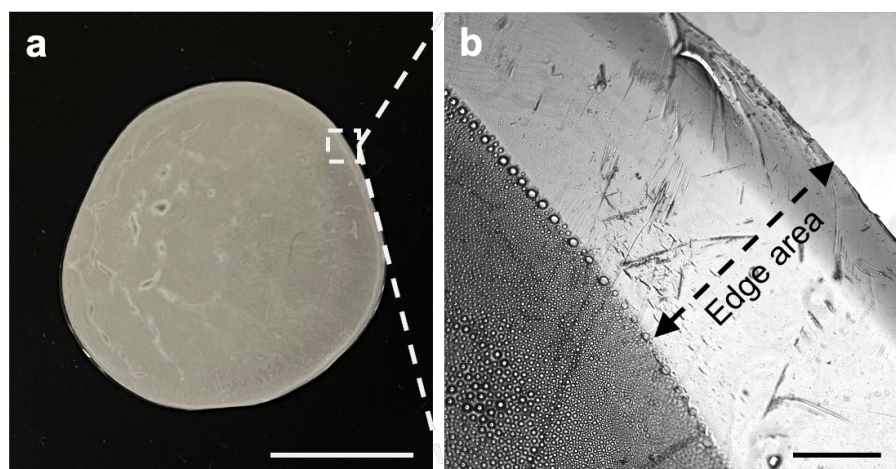
M13+HER262+BSA+GA microgel suspension, and representative antibiotics (ciprofloxacin and gentamicin) with different concentration on *E. coli* O157:H7 and BL21 lawns, respectively. Concentration gradient: Phage: 20×, 10×, and 1× of phage suspension prepared by the protocol. Ciprofloxacin and gentamicin: 20×, 10×, and 1× of minimal inhibitory concentration (MIC) against *E. coli* O157:H7 (Ciprofloxacin MIC: 0.03 $\mu\text{g mL}^{-1}$; Gentamicin MIC: 0.5 $\mu\text{g mL}^{-1}$).



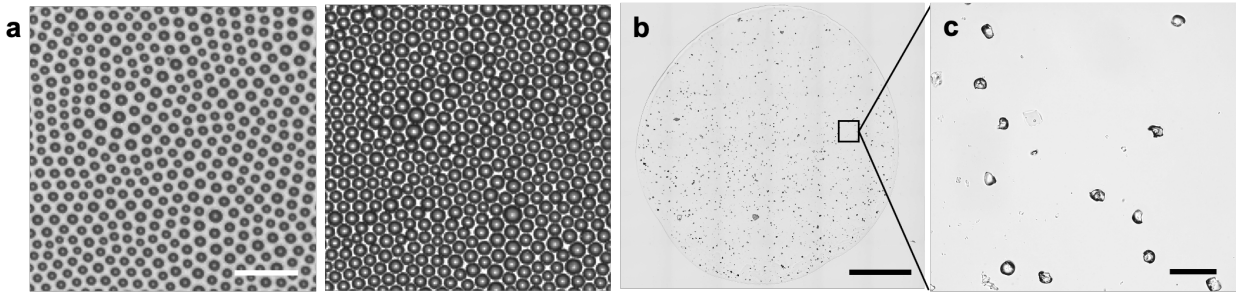
Supplementary Figure 3. Desiccation-sensitivity of phage M13, HER262 and T7. Titer count of phage M13, HER262 and T7 before (n=3 independent experiments for each type of phage) and after 1-h desiccation. (n=6 independent experiments for each type of phage) (M13: ***p=0.0005; HER262 and T7: ****p<0.0001). Data are presented as mean±SD with all data points. Statistical significance is derived from unpaired t-test. Image adapted with permission from ref.¹, Nature Portfolio.



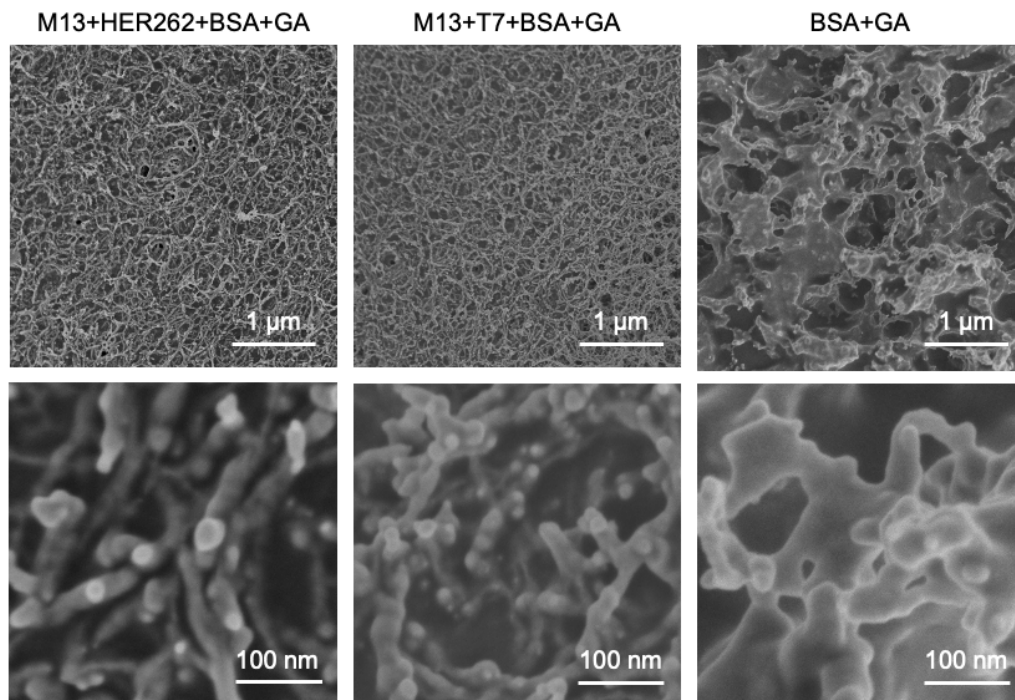
Supplementary Figure 4. Design of the chamber for the preparation of honeycomb films. a. Photograph of our transparent resinous chamber with size markings. **b.** Photograph of the transparent lid with an open-ended inlet (inner width: 4 mm) for adding polystyrene solution. The optional additional inlet can be used for preparing two films simultaneously.



Supplementary Figure 5. Edge area of the honeycomb films shows no micropores. a. Photograph of a honeycomb film. Scale bar: 1 cm. **b.** Bright field image of the framed area in panel a, where the edge area of honeycomb film (indicated by arrow) has no micropores. Scale bar: 50 μm .

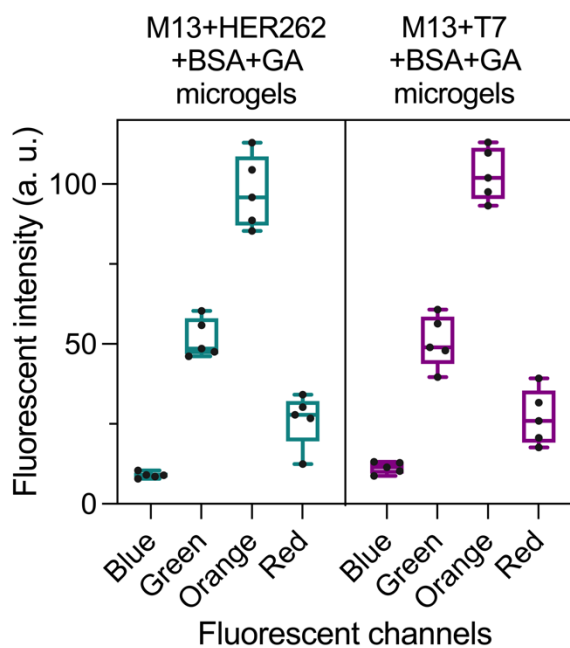


Supplementary Figure 6. Optical microscopy characterization of honeycomb films and microgels. **a**, Optical microscope images of the micropores on a honeycomb film under reflection mode and transmission mode respectively. Scale bar: 50 μm . **b**, Bright field image of 5 μL of phage microgel suspension. Scale bar: 1 mm. **c**, Zoomed-in bright field image of **b** showing free-stand microgels, isolated from the polystyrene template. Scale bar: 100 μm . **b-c** adapted with permission from ref.¹, Nature Portfolio.

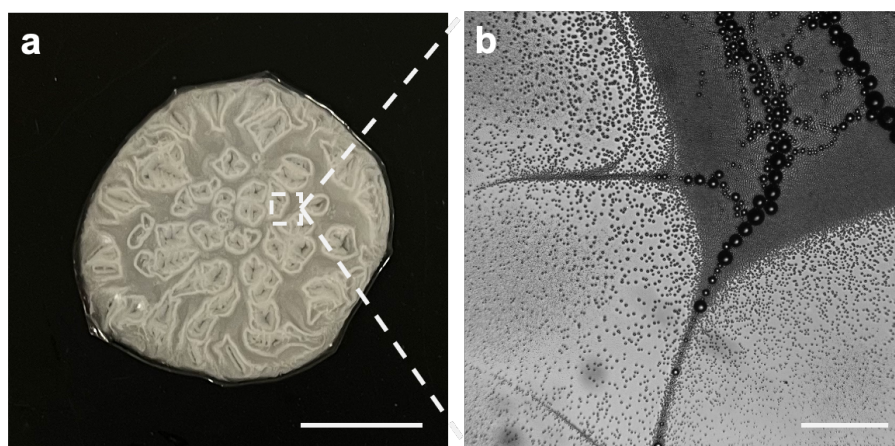


Supplementary Figure 7. FE-SEM images of the nanostructure on the surface of M13+HER262+BSA+GA, M13+T7+BSA+GA microgels, respectively. The images in the

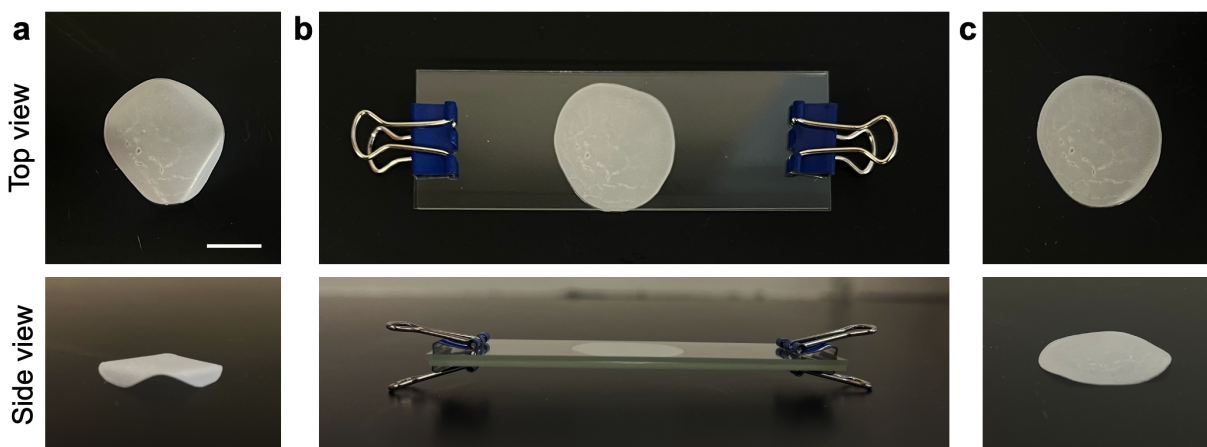
bottom row are zoomed-in versions of the corresponding top images. Image adapted with permission from ref.¹, Nature Portfolio.



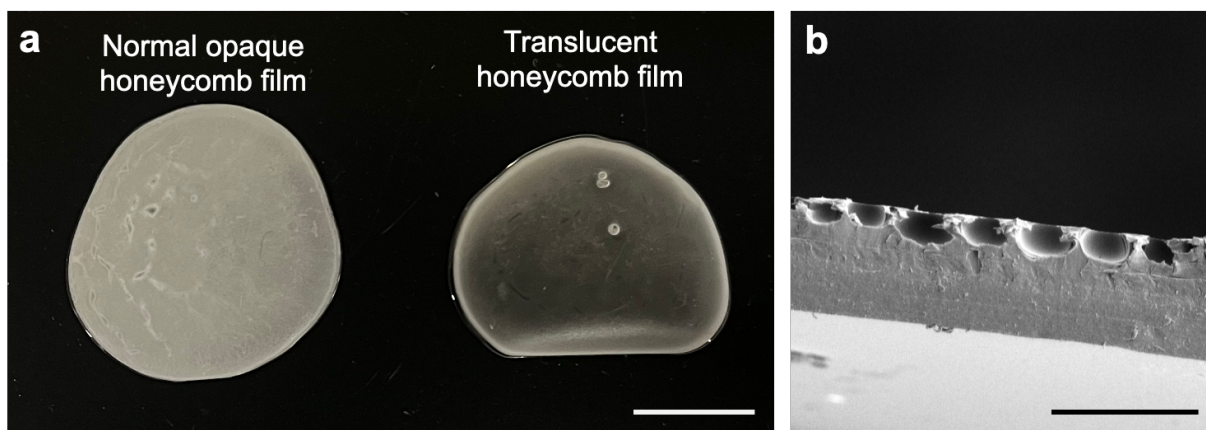
Supplementary Figure 8. Fluorescence intensity of M13+HER262+BSA+GA, M13+T7+BSA+GA microgels imaged under four different channels. Green channel: microgels excited at 465 nm and imaged using a $\lambda = 515$ nm optical filter. Orange channel: microgels excited at 528 nm and imaged using a $\lambda = 590$ nm optical filter. Red channel: microgels excited at 625 nm and imaged using a $\lambda = 670$ nm optical filter. Box plots show minimum to maximum (whiskers), 25–75% (box), median (band inside) with all data points. a.u. arbitrary unit. $n = 5$ microgels per fluorescence channel. Blue channel: microgels excited at 340 nm and imaged using a $\lambda = 435$ nm optical filter.



Supplementary Figure 9. Formation of honeycomb films with disordered micropores. **a.** Photograph of a honeycomb film prepared under external air interference. Scale bar: 1 cm. **b.** Bright field image of the the framed area in panel **a**, where micropores do not exhibit homogenous size and ordered arrangement. Scale bar: 300 μm .



Supplementary Figure 10. Process of turning crimped honeycomb film flat. **a.** Photographs of a crimped honeycomb film. **b.** Photographs of the film placing between two glass slides and secured with a clamp. **c.** Photographs of the flat honeycomb film after placing in the oven at 50 $^{\circ}\text{C}$ for 30 mins. Scale bar: 1 cm.



Supplementary Figure 11. Formation of a translucent honeycomb film. **a.** Photograph of a honeycomb film which was taken out of the humid chamber before solidifying (translucent) comparing to a normal honeycomb film (opaque). Scale bar: 1 cm. **b.** Cross-sectional SEM image of the translucent honeycomb film showing shallower pores comparing to **Fig. 2e**. Scale bar: 50 μm .

Reference

1. Tian, L. *et al.* Self-assembling nanofibrous bacteriophage microgels as sprayable antimicrobials targeting multidrug-resistant bacteria. *Nat. Commun.* **13**, 7158 (2022).